^{18}F-Fluciclovine PET Imaging of Glutaminase Inhibition in Breast Cancer Models

Rong Zhou, Hoon Choi, Jianbo Cao, Austin Pantel, Mamta Gupta, Hsiaoju S. Lee, and David Mankoff

Department of Radiology, University of Pennsylvania, Philadelphia, Pennsylvania

Aggressive cancers such as triple-negative breast cancer (TNBC) avidly metabolize glutamine as a feature of their malignant phenotype. The conversion of glutamine to glutamate by the glutaminase enzyme represents the first and rate-limiting step of this pathway and a target for drug development. Indeed, a novel glutaminase inhibitor (GLSi) has been developed and tested in clinical trials but with limited success, suggesting the potential for a biomarker to select patients who could benefit from this novel therapy. Here, we studied a nonmetabolized amino acid analog, ^{18}F-fluciclovine, as a PET imaging biomarker for detecting the pharmacodynamic response to GLSi. **Methods:** Uptake of ^{18}F-fluciclovine into human breast cancer cells was studied in the presence and absence of inhibitors of glutamine transporters and GLSi. To allow ^{18}F-fluciclovine PET to be performed on mice, citrate in the tracer formulation is replaced by phosphate-buffered saline. Mice bearing triple-negative breast cancer (TNBC) xenografts (HCC38, HCC1806, and MBA-MD-231) and estrogen receptor–positive breast cancer xenografts (MCF-7) were imaged with dynamic PET at baseline and after a 2-d treatment of GLSi (CB839) or vehicle. Kinetic analysis suggested reversible uptake of the tracer, and the distribution volume (V_D) of ^{18}F-fluciclovine was estimated by Logan plot analysis. **Results:** Our data showed that cellular uptake of ^{18}F-fluciclovine is mediated by glutamine transporters. A significant increase in V_D was observed after CB839 treatment in TNBC models exhibiting high glutaminase activity (HCC38 and HCC1806) but not in TNBC or MCF-7 exhibiting low glutaminase. Changes in V_D were corroborated with changes in GLS activity measured in tumors treated with CB839 versus vehicle, as well as with changes in V_D of ^{18}F-(2S,R4)-fluoroglutamine, which we previously validated as a measure of cellular glutamine pool size. A moderate, albeit significant, decrease in ^{18}F-FDG PET signal was observed in HCC1806 tumors after CB839 treatment. **Conclusion:** ^{18}F-fluciclovine PET has potential to serve as a clinically translatable pharmacodynamic biomarker of GLSi.

Key Words: ^{18}F-fluciclovine PET; triple-negative breast cancer; glutaminase; distribution volume; CB839

J Nucl Med 2023; 64:131–136
DOI: 10.2967/jnumed.122.264152

Reprogramming of energy metabolism has been recognized as a hallmark of cancer (*1*). Dysregulation of cellular metabolic pathways enables cancer cells to meet their energetic and biosynthetic needs but also provides opportunities to selectively target cancer cells while sparing normal tissues. Targeting such a cancer-specific metabolic signature could be useful for treating triple-negative breast cancer (TNBC), which lacks a subtype-specific treatment because of absence of the estrogen receptor, the progesterone receptor, and the human epidermal growth factor receptor 2. Glutaminolysis, the metabolic pathway of glutamine, is used by many aggressive cancers, including TNBC (*2,3*), and hence might be exploited for therapy. Conversion of glutamine to glutamate by the mitochondrial enzyme glutaminase represents the first and rate-limiting step in the pathway. In cancers, it is the kidney type rather than the liver type of glutaminase that is predominantly expressed. Highly potent and specific inhibitors of glutaminase (GLSi) have been developed. Several of these agents have shown promise in preclinical studies (*4–7*), and one agent, CB839 (Telaglenastat developed by Calithera Bioscience), has advanced into clinical trials. Although CB839 has been well tolerated in clinical trials, efficacy has been variable (*8–10*). These trials, though, did not include biomarkers to assess target impact and guide patient selection, potentially confounding the overall study results. Although enhanced glutamine metabolism is frequently observed in TNBC—more so than in other subtypes of breast cancer—individual TNBCs are highly heterogeneous and exhibit a wide range of glutaminase activity (*4*). As such, a method to evaluate the pharmacodynamic response of TNBC to GLSi would be highly valuable for patient selection in the clinical setting when glutaminase activity cannot be readily assessed.

Previous studies have elucidated an inverse relationship between glutaminase activity and glutamine pool size, providing a paradigm for imaging glutamine metabolism with amino acids analogs. Tumors with a high glutaminase activity have a low cellular glutamine concentration (pool size) accompanied by a high glutamate (the product of the glutaminase) level (*4*). Upon glutaminase inhibition, the cellular glutamine pool increases because of blockade of glutamine conversion to glutamate (*4,11*). It follows that such an increase in tumor cellular glutamine pool size can serve as a specific pharmacodynamic marker for GLSi.

Our approach toward measuring the change in tumor glutamine pool size relies on tracers that mimic bidirectional glutamine transport into and out of the cancer cell but are not metabolized by glutaminase. Under these conditions, and assuming stable kinetics for glutamine transport and metabolism over the course of the imaging study (~1 h), the PET signal will fit a single reversible tracer kinetic model (*12*) in which the distribution volume (V_D) provides a direct measure of intracellular glutamine concentration. We and others have previously shown that cellular uptake of glutamine analog ^{18}F-(2*S*,4*R*)4-fluoroglutamine (^{18}F-4F-glutamine) is mediated by the native glutamine transporters (*13*) but is a poor substrate for kidney-type glutaminase expressed in the tumor (*14,15*). Furthermore, in human breast cancer xenograft models, the V_D of ^{18}F-4F-glutamine PET or the tumor-to-blood ratio (T/B) 30–45 min after injection can serve as a pharmacodynamic marker of GLSi (*15,16*).

Received Mar. 23, 2022; revision accepted Jun. 21, 2022.
For correspondence or reprints, contact Rong Zhou (rongzhou@pennmedicine.upenn.edu) or David Mankoff (david.mankoff@pennmedicine.upenn.edu).
Published online Jun. 30, 2022.

^{18}F-4F-glutamine, however, is an investigational agent and has been reported to undergo defluorination (*17,18*), which might confound the PET signal and potentially mask bone disease, a common site of breast cancer metastasis. To overcome these limitations, we considered ^{18}F-fluciclovine (Axumin; Blue Earth Diagnostics), a metabolically inert analog of L-leucine (*16*), with uptake into cancer cells mediated by glutamine transporters (*19,20*). Hence, ^{18}F-fluciclovine may serve as an alternative tracer for measuring glutamine pool size and the impact of GLSi. Although ^{18}F-fluciclovine has been studied under investigational settings for breast cancer (*21,22*), its utility as a metabolic marker has not been established. Here, we performed a proof-of-principle study of ^{18}F-fluciclovine as a pharmacodynamic marker for GLSi, comparing with ^{18}F-4F-glutamine by employing the same tumor models and analysis methods (*15,16*). We were able to show that the uptake of ^{18}F-fluciclovine is mediated by glutamine transporters; ^{18}F-fluciclovine has reversible kinetics that reflect cellular glutamine pool size, and short-term exposure to GLSi leads to significant increases in ^{18}F-fluciclovine V_D similar to those in ^{18}F-4F-glutamine.

MATERIALS AND METHODS

Materials

^{18}F-fluciclovine was provided by Blue Earth Diagnostics. A vehicle solution of 25% (w/v) hydroxypropyl-β-cyclodextrin in 10 mM citrate (pH 2) (*15*) and CB839 formulated in the vehicle or in dimethyl sulfoxide were provided by Calithera Biosciences. ^{18}F-(2*S*,4*R*)4-fluoroglutamine (*15*) and ^{18}F-FDG were produced at the PET Center, University of Pennsylvania.

The following reagents, assay kits, and cell lines were purchased: ion-exchange resin columns (catalog no. 731621) from Bio-Rad; a citrate assay kit (catalog no. MAK057), L-glutamine, GPNA (L-γ-glutamyl-*p*-nitroanilide), and BCH (2-aminobicyclo-(*1,2*)-heptane-2-carboxylic acid) from Sigma; syringe filters (catalog no. 09-720-3) and 96-well strips plate (catalog no. 07-200-97) from Fisher Scientific; human TNBC (HCC1806, HCC38, and MDA-MB-231) and estrogen receptor–positive (MCF-7) breast cancer cell lines from American Type Culture Collection. The cell lines were authenticated using the short-tandem-repeat DNA profiling method and were used within 6 mo from the date of purchase. Cells were maintained in complete culture medium consisting of RPMI-1640 (catalog no. 25-506; GenClone) supplemented with 10% HyClone fetal bovine serum without antibiotics.

Removal of Citrate from the Formulation of ^{18}F-Fluciclovine

After the deionized water was released from the column resin, the column was loaded with the tracer solution (~0.9 mL) provided by the vendor. An equal volume (0.9 mL) of phosphate-buffered saline (PBS) was added to the column, and the eluted solution was collected (~0.9 mL in ~1–2 min) in a sterile test tube. This was repeated by adding PBS (0.9 mL) and collecting the elution in another sterile test tube. The ^{18}F activity in the eluted solution was estimated by a dose calibrator (CRC-7; Capintec), whereas the pH and residual citrate in the solution were assessed by pH test strips and citrate assay, respectively.

In Vitro Cell Uptake of ^{18}F-Fluciclovine

Breast cancer lines HCC38, HCC1806, and MCF-7 were included. Cells (30,000, 25,000, and 30,000 cells per well for HCC38, HCC1806, and MCF-7, respectively) were seeded in a 96-well strip plate and incubated overnight in complete culture medium. To study tracer uptake, the cells were incubated in PBS containing 5 mM glucose and 100 μM glutamine to which ^{18}F-fluciclovine (~300,000 cpm/well) was added at time zero. To test whether ^{18}F-fluciclovine uptake is mediated by glutamine transporters, glutamine (5 mM), GPNA (1 mM), BCH (10 mM), or dimethyl sulfoxide control (0.05%) in PBS containing 5 mM glucose was added at time zero. After a specified incubation time (5, 15, 30, 60, and 120 min), supernatant was aspirated, and the wells were washed twice with cold PBS. After washing, activity in each well was counted on a γ-counter (2470 Wizard2; Perkin Elmer), and the amount of protein was estimated by the Lowry method (*15*). To inhibit glutaminase activity, the cells were incubated in culture medium containing 1 μM CB839 or 0.05% dimethyl sulfoxide as a control for 24 h before cell uptake studies because cellular metabolite concentration remains unchanged during 24 h of incubation with CB839 (*4*); the drug was present during incubation with the radiotracer.

Human Breast Cancer Xenograft Models and Treatment with GLSi (CB839)

All animal procedures were approved by the institutional animal care and use committee of the University of Pennsylvania. NCR athymic nu/nu mice (female, 7 wk old) were purchased from Charles River. To establish the human breast cancer xenografts, 1×10^6 HCC1806 cells in 100 μL of PBS and 5×10^6 MCF-7 or HCC38 cells in 150 μL of Matrigel (Corning) solution (1:1 mixed with PBS) were subcutaneously inoculated into the right flank of the mice. Tumor size was measured by a reader who was blinded to the PET image analysis using a caliper in 2 orthogonal directions (*a* and *b,* with *b* being the shorter dimension) using the formula volume = $(1/6) \times \pi \times a \times b^2$. CB839 formulated in the vehicle solution (*15*) was administered via oral gavage (200 mg/kg twice daily) for 2 d; control mice received the same volume of vehicle solution (~0.25 mL).

Quantification of Glutaminase Activity in Cells and Tumor Tissues

To process cells for glutaminase activity, a pellet of 10 million cells was suspended in 1 mL of homogenization buffer (50 mM tris-acetate, pH 8.6; 15 mM K_2HPO_4; 150 mM KCl; 0.25 mM ethylenediaminetetraacetic acid; and 1 mM dithiothreitol including 1x complete protease inhibitor) in a 2-mL tube containing ceramic beads (Bertin Instruments). Tumor tissue was clamp-frozen in liquid nitrogen upon euthanasia of the mouse and kept in a −80°C freezer. The homogenization buffer (as above) was added to the weighed tissue (v/w = 10/1) in a 2-mL tube containing ceramic beads.

Cell or tissue samples were homogenized at 4°C using a Precellys Evolution homogenizer equipped with Cryolys Evolution (Bertin Instruments). The supernatant was removed and passed through a gel filtration spin column (Zeba spin desalting column; Fisher Scientific). The filtered supernatant and substrates which include glutamate dehydrogenase, nicotinamide adenine dinucleotide phosphate, and glutamine were mixed to start the enzymatic reaction generating reduced nicotinamide adenine dinucleotide phosphate, which was detected by fluorescence (excitation wavelength, 340 nm/emission wavelength, 460 nm) and recorded every minute for 15 min at 25°C in a microplate reader (SpectraMax M5; Molecular Devices). Specific activity was calculated from the background-corrected velocity (nmol reduced nicotinamide adenine dinucleotide phosphate/min) divided by the amount of protein. A standard curve was produced using pure glutaminase (catalog no. G8880; Sigma).

In Vivo PET/CT Imaging and Analysis of Dynamic PET Images

In vivo PET/CT was performed on the Molecubes modular system (Molecubes Corp.) before and after 4 doses of CB839 or vehicle treatment. Approximately 7,400–9,250 kBq (200–250 μCi) of ^{18}F-fluciclovine in 0.2 mL was injected into the tail vein catheter, and a 45-min dynamic PET scan was started immediately and followed by a 2-min CT scan. The dynamic PET data were reconstructed with a temporal resolution of 10 s/frame × 6 frames, 1 min/frame × 9 frames, and 5 min/frame × 7 frames. ^{18}F-FDG PET imaging was applied to a separate cohort of mice subjected to the same treatment. After 4 h of fasting, the mice were

injected with 3,700 kBq (100 μCi) of ^{18}F FDG and allowed to recover from the anesthesia. Two hours after ^{18}F FDG injection, the mice were anesthetized and underwent a 15-min static PET scan.

PET data were analyzed using PMOD software, version 3.711. A spheric region of interest (ROI) equal to an eighth the volume of the tumor (measured by caliper before imaging) was placed over the hottest region of the tumor while avoiding activities from nearby bones by referencing the CT image. The time–activity curve of the tumor was then obtained from the ROI. To measure the activity in the blood, a 2 × 2 × 2 mm cubic region of interest was placed over the left ventricle of the heart of the mouse by referencing the CT image. The image analysis methods used in this study match those of ^{18}F-4F-glutamine (*15,16*), including the tumor ROI size. Time–activity curves for the blood and tumor were imported to the general kinetic modeling tool (PKIN) of PMOD for analyses. The preliminary analyses showed that the kinetic data fit both a 1- and a 2-compartment model, but the 2-compartment model fit returned a small k_3 value (0–0.02/min), consistent with a reversible uptake of the tracer as reported earlier for ^{18}F-4F-glutamine in mice (*16*) and patients (*23*). Henceforward, given reversible uptake, the Logan plot (*24*), a simplified graphical method based on compartment model analysis, was used to estimate the tracer V_D of the tumor.

Statistical Analysis

Data are presented as mean ± SD (represented by error bars). Statistical tests were performed using GraphPad Prism, version 6. A 2-sided Student *t* test was used to evaluate difference between 2 groups, with α set at 0.05.

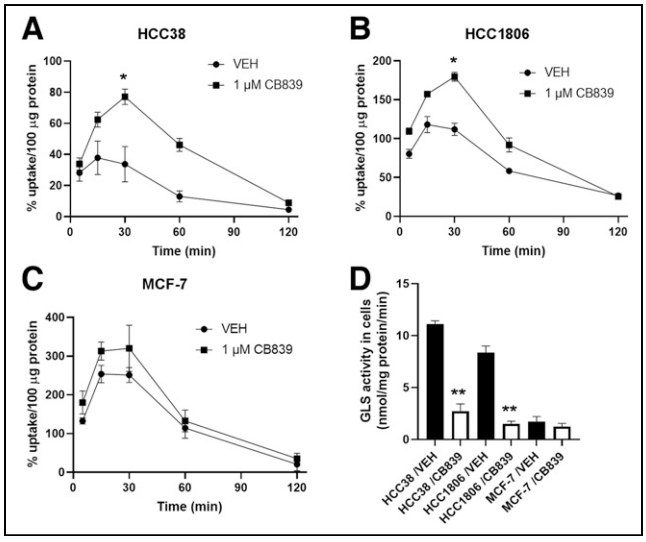

FIGURE 2. Cellular uptake of ^{18}F-fluciclovine and glutaminase activity in TNBC and estrogen receptor–positive breast cancer cells. Dynamic uptake profile of HCC38 (A), HCC1806 (B), and MCF-7 (C) cells is shown, as well as glutaminase activities after CB839 or vehicle treatment (D). Error bars are SD. *P* values compare CB839 vs. vehicle group in D: HCC38/4.58×10^{-5}, HCC1806/7.12×10^{-5}, MCF-7/0.22. In A–C, each point in graph represents mean ± SD from 4 replicates; in D, each bar represents mean ± SD from 3 mice. VEH = vehicle.

RESULTS

Citrate assay results demonstrated that the column filtration protocol almost completely removed citrate and that more than 80% of ^{18}F radioactivity was recovered in eluted PBS with an activity concentration of 170–185 MBq (4.6–5 mCi)/mL, suitable for injection into mice (Supplemental Figs. 1A and 1B; supplemental materials are available at http://jnm.snmjournals.org). The citrate-replaced tracer solution appeared safe, without causing weight loss over 7 d (Supplemental Fig. 1C).

To assess whether ^{18}F-fluciclovine uptake is mediated by glutamine transporters, tracer uptake was measured in the presence and absence of cold glutamine and pharmacologic inhibitors of alanine-serine-cysteine transporter 2 (GPNA) and large neutral amino acid transporter 1 (BCH) as shown in Fig. 1. ^{18}F-fluciclovine uptake was blocked approximately 100%, 82%, and 56% by cold glutamine, BCH, and GPNA, respectively, at 30 min compared with the control ($P < 0.00001$ for all).

We then evaluated the impact of GLSi on ^{18}F-fluciclovine uptake in human TNBC (HCC38 and HCC1806) and in estrogen receptor–positive breast cancer (MCF-7) cells, which exhibit distinct glutaminase activity (HCC38 > HCC1806 ≫ MCF-7). Consistent with a reversible uptake pattern, the uptake peaked at around 30 min, followed by washout as shown in Figures 2A–2C: at 30 min, tracer uptake was significantly higher in CB839-treated HCC38 and HCC1806 cells than in vehicle controls, but the difference was minimal in MCF-7 cells. Corroborated by glutaminase activities in the presence and absence of GLSi (Fig. 2D), these data suggest that inhibition of active glutaminase results in a large increase in glutamine pool size that is reflected in significant increases in ^{18}F-fluciclovine uptake in these cells.

Logan plots of PET data acquired before treatment revealed a distinct slope (V_D) for the 3 models (HCC38 < HCC1806 < MCF-7, Supplemental Fig. 2A), inverse to their glutaminase activity. In vivo static PET images (last frame) revealed an increase in ^{18}F-fluciclovine PET signal in HCC38 and HCC1806 tumor after GLSi treatment (Supplemental Fig. 2B). Changes in V_D were then examined: in the HCC1806 model, a significant increase in V_D was observed after a short course (2 d) of CB839 treatment (pretreatment vs. posttreatment V_D: 1.24 ± 0.26 vs. 2.05 ± 0.26, $P = 0.0055$, paired *t* test, $n = 6$, Fig. 3A); for comparison, the V_D of the vehicle control group showed a nonsignificant decrease (pretreatment vs. posttreatment V_D: 1.33 ± 0.24 vs. 1.05 ± 0.20, $P = 0.24$, paired *t* test, $n = 7$). Changes in T/B shown in Supplemental Figure 3 are consistent with changes in V_D. Two additional TNBC models were examined in fewer mice: in HCC38 model (high glutaminase), V_D was increased by an average of 23% after CB839 ($n = 3$), compared with a 37% decrease after vehicle

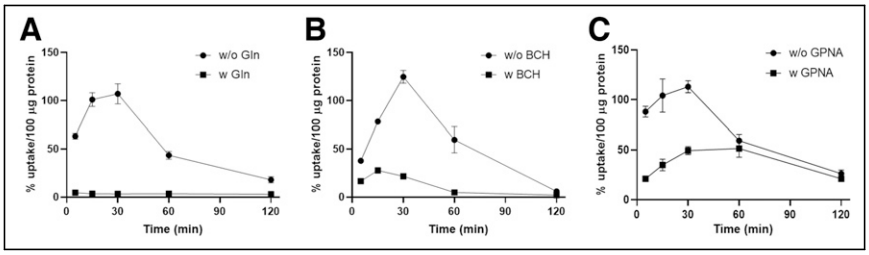

FIGURE 1. Cellular uptake of ^{18}F-fluciclovine is mediated by glutamine transporters. Uptake into HCC1806 cells was blocked by excess of glutamine (A), BCH (B), or GPNA (C). Glutamine (5 mM), BCH (10 mM), or GPNA (1 mM) was added at time zero to incubation medium made of PBS containing 5 mM glucose (final concentration of these reagents are specified in parentheses). Each point in graph represents mean ± SD from 4 replicates. Gln = glutamine.

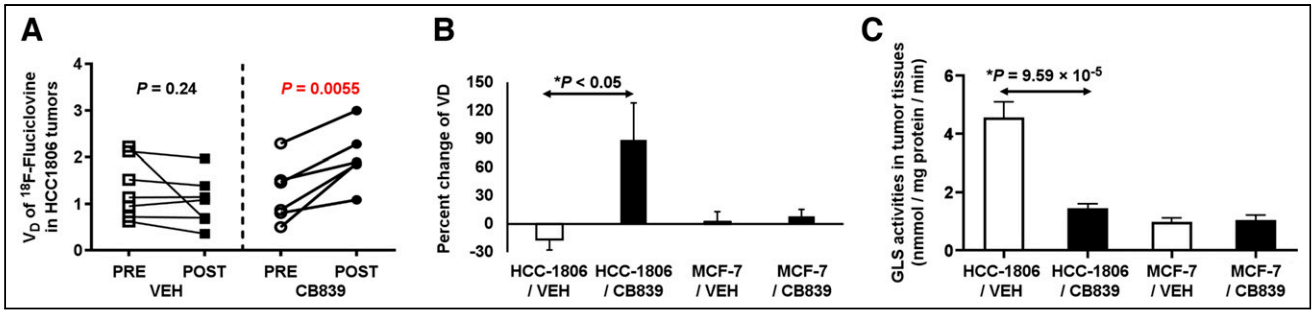

FIGURE 3. ^{18}F-fluciclovine V_D before and after GLSi treatment and change in V_D induced by GLSi or vehicle treatment and tumor glutaminase activities in TNBC and estrogen receptor–positive BC. (A) Pre- and posttreatment V_D of individual mice bearing HCC1806 tumor enrolled in vehicle-treated group (n = 7) or CB839-treated group (n = 6). (B) Percentage change in V_D [100* (Posttreatment VD-Pretreatment VD)/Pretreatment VD] of vehicle-treated and CB839-treated groups for HCC1806 tumors (n = 7 and 6, respectively) and for MCF-7 tumors (n = 5 and 4, respectively). (C) Glutaminase activities of vehicle- and CB839-treated tumors (HCC1806 after CB839: 1.46 ± 0.13 [n = 4]; HCC1806 after vehicle: 4.56 ± 0.44 [n = 3]; MCF-7 after CB839: 1.07 ± 0.17 [n = 5]; MCF-7 after vehicle: 0.99 ± 0.12 [n = 3].

treatment (n = 2); in MDA-MB-231 model (low glutaminase activity), V_D was decreased by 5% and 7% after CB839 treatment (n = 1) and vehicle treatment (n = 2), respectively.

We further compared the V_D of ^{18}F-fluciclovine versus that of ^{18}F-4F-glutamine PET (Fig. 4): in the HCC1806 model, a large increase in V_D (slope of Logan plot) was observed in both ^{18}F-fluciclovine and ^{18}F-4F-glutamine after CB839 treatment compared with baseline (Figs. 4A–4B); in MCF-7, only a modest change in the slope was detected (Figs. 4C–4D). In some mice, an overall increase in ^{18}F PET signal was observed after CB839 treatment, likely due to an increase in plasma glutamine level after CB839 exposure (*15*), leading to decreased clearance of ^{18}F-4F-glutamine or ^{18}F-fluciclovine. Groupwise, CB839 treatment led to an increase in V_D (89% ± 39%), compared with a decrease (−16% ± 11%) after vehicle treatment in the HCC1806 model (Fig. 3B, $P < 0.05$); modest changes were observed in MCF-7 tumors after CB839 or vehicle treatment (P = 0.6). These values compare favorably with those of ^{18}F-4F-glutamine PET: T/B estimated directly from PET images acquired from 30 to 45 min is a proxy of V_D and was increased by 34% ± 14% in HCC1806 tumors after CB839, compared with −11% ± 24% after vehicle treatment (*15*), and T/B and V_D were highly correlated (r^2 = 0.92) (*16*). Glutaminase enzymatic activity measured from tumor tissues revealed a large, 3-fold, reduction in HCC1806 tumors after CB839 treatment compared with vehicle controls, whereas there was no significant change in MCF-7 tumors (Fig. 3C).

Finally, we tested whether ^{18}F-FDG PET can detect responses to CB839 treatment (Supplemental Figs. 4A–4B). A moderate albeit significant decrease in ^{18}F-FDG PET signal (percent of injected dose per gram, %ID/g) was observed in HCC1806 tumors after CB839 treatment (pretreatment vs. posttreatment %ID/g: 2.94 ± 0.24 vs. 2.29 ± 0.21, n = 11, $P < 0.05$); a decrease was also observed in the vehicle group, but it was not significant (pretreatment vs. posttreatment %ID/g: 3.47 ± 0.59 vs. 2.47 ± 0.016, n = 5, P = 0.31).

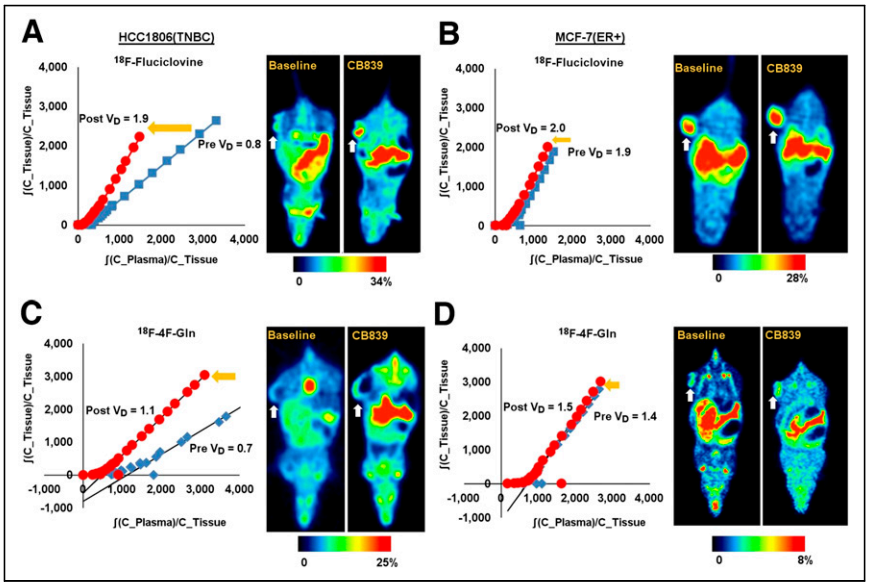

FIGURE 4. Comparison of ^{18}F-fluciclovine vs. ^{18}F-4F-glutamine PET for detecting pharmacodynamic responses to GLSi. Shown are Logan plots and PET images of ^{18}F-Fluciclovine from representative mice bearing HCC1806 (A) and MCF-7 tumor (B) at baseline and post CB839 treatment. Logan plots and PET images of ^{18}F-4F-Gln from HCC1806 (C) and MCF-7 (D) bearing mice are shown for the same treatment. Sample sizes for ^{18}F-4F-glutamine study were reported earlier (*15*), whereas those for ^{18}F-fluciclovine are described in Figure 3. Same color scale (based on percentage of maximum signal intensity) is applied to both pretreatment and posttreatment PET images.

DISCUSSION

Blockade of ^{18}F-fluciclovine cell uptake by glutamine, as well as by pharmacologic inhibitors of large neutral amino acid transporter 1 (BCH) and alanine-serine-cysteine transporter 2 (GPNA), confirms that ^{18}F-fluciclovine enters the cells via glutamine transporters. Indeed, prior studies have shown that alanine-serine-cysteine transporter 2 mediates glutamine uptake in many cancer cells (*13,25*), including TNBC (*26*). In vivo PET studies demonstrated a large increase in V_D in TNBC models exhibiting high glutaminase activity (HCC1806 and HCC38) after a short course of GLSi treatment. However, no increase was detected after vehicle (control)

treatment or in models exhibiting low glutaminase activity (MDMBA-231 and MCF-7). These results are corroborated by glutaminase activities in tumor specimens and support that increased ^{18}F-fluciclovine uptake reflects inhibition of active glutaminase. The ability of ^{18}F-fluciclovine to report a pharmacodynamic response to GLSi enables early detection of target engagement and prediction of GLSi futility if the tumor fails to demonstrate an alteration in tracer uptake kinetics in response to the drug. This approach using a target-specific drug with short-term exposure as a perturbagen, and a mechanistically matched tracer, has been tested in other scenarios, including human studies of drug efflux inhibitors (*27*), estrogen receptor agonists (*28*), and estrogen receptor blockade (*29*). It is possible, and likely, that longer exposure may lead to differences in results, as was seen in studies that tested residual ^{18}F-fluciclovine as a marker of resistant, viable tumor (*22*). The time course of the increase in tumor glutamine pool size and matched alteration in ^{18}F-fluciclovine kinetics will need to be studied in future preclinical and clinical studies testing ^{18}F-fluciclovine as a marker to guide glutaminase-targeted therapy.

Our data also revealed that ^{18}F-FDG PET is not a sensitive marker for GLSi, likely because glucose uptake or metabolism is not directly impacted by a short exposure to GLSi (*4*). ^{18}F-FDG can likely serve as a marker of cell viability or death over extended periods, as it does for a variety of cancer cell types and treatments (*30*).

The approach of using amino acid analogs that are not metabolized or substrates for biosynthesis differs fundamentally from that of metabolized tracers such as ^{11}C-glutamine (*31*), which participates in biosynthesis and is metabolized through glutaminolysis to produce ^{11}C-CO_2 and radiolabeled metabolites (e.g., ^{11}C-glutamate), leading to a complex distribution of the radiolabel that must be accounted for. Although ^{11}C-glutamine has recently been studied in human subjects (*32*), the complexity behind the ^{11}C PET signal would be a challenge for proper interpretation of PET signal changes and widespread clinical adoption. In contrast, complexity is mitigated by nonmetabolized tracers, such as ^{18}F-fluciclovine, whereby enzymatic activity and drug effect are inferred from changes in pool size (*33,34*). The favorable comparison of the V_D of ^{18}F-fluciclovine versus ^{18}F-4F-glutamine (Fig. 4) strongly suggests that clinical translation could be facilitated by ^{18}F-fluciclovine because of its superior chemical stability, widespread consensus regarding lack of metabolism (*35*), and commercial availability.

Our study had a few limitations. First, whereas changes in V_D observed in 2 other TNBC models (HCC38 and MDA-MB-231) were consistent with the expectation, their sample sizes were relatively small. However, a primary goal of this study was to compare the V_D of ^{18}F-fluciclovine with that of ^{18}F-4F-glutamine previously estimated in HCC1806 and MCF-7 models (*15,16*). Second, tumor glutamine pool sizes were not directly quantified; in a previous study, however, glutamine concentration was measured independently by proton nuclear magnetic resonance technique in HCC1806 and MCF-7 tumors after the same treatment regimen, and a strong correlation was found between tumor glutamine pool size and T/B, a proxy of V_D (*15*).

CONCLUSION

The findings of the current study suggest that ^{18}F-fluciclovine PET provides a tool for assessing tumor glutamine pool size and can serve as a pharmacodynamic marker for GLSi (such as CB839). The favorable biochemical properties and established availability of this tracer make it an attractive candidate for future human translation.

DISCLOSURE

This study was supported by R21CA198563, R01CA211337, and Komen SAC130060. 18F-fluciclovine and CB839 were generously provided by Blue Earth Diagnostics and Calithera, respectively. No other potential conflict of interest relevant to this article was reported.

ACKNOWLEDGMENTS

We are grateful to Dr. Varsha Viswanath and Daniel Kranseler for assistance in data processing and to Drs. Karen Linder and Hamed Hossein of Blue Earth Diagnostics for insightful discussions.

KEY POINTS

QUESTION: Can ^{18}F-fluciclovine PET report the pharmacodynamic effect of GLSi in glutaminase-active breast cancers?

PERTINENT FINDINGS: ^{18}F-fluciclovine is taken up in breast cancer cells via glutamine transporters and is not metabolized; thus, ^{18}F-fluciclovine is capable of tracking glutamine pool size. In human breast cancer models of differential glutaminase activity, a significant increase in ^{18}F-fluciclovine V_D was observed after GLSi treatment in tumor models exhibiting high glutaminase activity but not in those with low activity.

IMPLICATIONS FOR PATIENT CARE: A ^{18}F-fluciclovine PET marker might provide information that can help select patients for treatment targeting glutamine metabolism such as GLSi.

REFERENCES

1. Hanahan D, Weinberg RA. Hallmarks of cancer: the next generation. *Cell.* 2011; 144:646–674.
2. DeBerardinis RJ, Cheng T. Q's next: the diverse functions of glutamine in metabolism, cell biology and cancer. *Oncogene.* 2010;29:313–324.
3. DeBerardinis RJ, Lum JJ, Hatzivassiliou G, Thompson CB. The biology of cancer: metabolic reprogramming fuels cell growth and proliferation. *Cell Metab.* 2008;7: 11–20.
4. Gross MI, Demo SD, Dennison JB, et al. Antitumor activity of the glutaminase inhibitor CB-839 in triple-negative breast cancer. *Mol Cancer Ther.* 2014;13: 890–901.
5. Boysen G, Jamshidi-Parsian A, Davis MA, et al. Glutaminase inhibitor CB-839 increases radiation sensitivity of lung tumor cells and human lung tumor xenografts in mice. *Int J Radiat Biol.* 2019;95:436–442.
6. Momcilovic M, Bailey ST, Lee JT, et al. Targeted inhibition of EGFR and glutaminase induces metabolic crisis in EGFR mutant lung cancer. *Cell Rep.* 2017;18: 601–610.
7. Hoerner CR, Chen VJ, Fan AC. The 'Achilles heel' of metabolism in renal cell carcinoma: glutaminase inhibition as a rational treatment strategy. *Kidney Cancer.* 2019;3:15–29.
8. Meric-Bernstam F, Tannir NM, Mier JW, et al. Phase 1 study of CB-839, a small molecule inhibitor of glutaminase (GLS), alone and in combination with everolimus (E) in patients (pts) with renal cell cancer (RCC) [abstract]. *J Clin Oncol.* 2016;34(suppl):4568.
9. Zhao Y, Feng X, Chen Y, et al. 5-fluorouracil enhances the antitumor activity of the glutaminase inhibitor CB-839 against PIK3CA-mutant colorectal cancers. *Cancer Res.* 2020;80:4815–4827.
10. Wang Z, Liu F, Fan N, et al. Targeting glutaminolysis: new perspectives to understand cancer development and novel strategies for potential target therapies. *Front Oncol.* 2020;10: 589508.

11. Kung HN, Marks JR, Chi JT. Glutamine synthetase is a genetic determinant of cell type-specific glutamine independence in breast epithelia. *PLoS Genet.* 2011;7: e1002229.
12. Pantel AR, Viswanath V, Muzi M, Doot RK, Mankoff DA. Principles of tracer kinetic analysis in oncology, part II: examples and future directions. *J Nucl Med.* 2022;63:514–521.
13. Venneti S, Dunphy MP, Zhang H, et al. Glutamine-based PET imaging facilitates enhanced metabolic evaluation of gliomas in vivo. *Sci Transl Med.* 2015;7:274ra17.
14. Jeitner TM, Kristoferson E, Azcona JA, et al. Fluorination at the 4 position alters the substrate behavior of L-glutamine and L-glutamate: implications for positron emission tomography of neoplasias. *J Fluor Chem*. 2016;192:58–67.
15. Zhou R, Pantel AR, Li S, et al. [^{18}F](2*S*,4*R*)4-fluoroglutamine PET detects glutamine pool size changes in triple-negative breast cancer in response to glutaminase inhibition. *Cancer Res.* 2017;77:1476–1484.
16. Viswanath V, Zhou R, Lee H, et al. Kinetic modeling of ^{18}F-(2*S*,4*R*)4-fluoroglutamine in mouse models of breast cancer to estimate glutamine pool size as an indicator of tumor glutamine metabolism. *J Nucl Med.* 2021;62:1154–1162.
17. Ploessl K, Wang L, Lieberman BP, Qu W, Kung HF. Comparative evaluation of ^{18}F-labeled glutamic acid and glutamine as tumor metabolic imaging agents. *J Nucl Med.* 2012;53:1616–1624.
18. Dunphy MPS, Harding JJ, Venneti S, et al. In vivo PET assay of tumor glutamine flux and metabolism: in-human trial of ^{18}F-(2*S*,4*R*)-4-fluoroglutamine. *Radiology.* 2018;287:667–675.
19. Okudaira H, Nakanishi T, Oka S, et al. Kinetic analyses of trans-1-amino-3-[^{18}F]fluorocyclobutanecarboxylic acid transport in *Xenopus laevis* oocytes expressing human ASCT2 and SNAT2. *Nucl Med Biol.* 2013;40:670–675.
20. Savir-Baruch B, Zanoni L, Schuster DM. Imaging of prostate cancer using fluciclovine. *PET Clin.* 2017;12:145–157.
21. Tade FI, Cohen MA, Styblo TM, et al. *Anti*-3-^{18}F-FACBC (^{18}F-fluciclovine) PET/CT of breast cancer: an exploratory study. *J Nucl Med.* 2016;57:1357–1363.
22. Ulaner GA, Goldman DA, Corben A, et al. Prospective clinical trial of ^{18}F-fluciclovine PET/CT for determining the response to neoadjuvant therapy in invasive ductal and invasive lobular breast cancers. *J Nucl Med.* 2017;58:1037–1042.
23. Scott NP, Teoh EJ, Flight H, et al. Characterising ^{18}F-fluciclovine uptake in breast cancer through the use of dynamic PET/CT imaging. *Br J Cancer.* 2022;126: 598–605.
24. Logan J, Fowler JS, Volkow ND, et al. Graphical analysis of reversible radioligand binding from time—activity measurements applied to [*N*-^{11}C-methyl]-(−)-cocaine PET studies in human subjects. *J Cereb Blood Flow Metab.* 1990;10:740–747.
25. Schulte ML, Fu A, Zhao P, et al. Pharmacological blockade of ASCT2-dependent glutamine transport leads to antitumor efficacy in preclinical models. *Nat Med.* 2018;24:194–202.
26. van Geldermalsen M, Wang Q, Nagarajah R, et al. ASCT2/SLC1A5 controls glutamine uptake and tumour growth in triple-negative basal-like breast cancer. *Oncogene.* 2016;35:3201–3208.
27. Sasongko L, Link JM, Muzi M, et al. Imaging P-glycoprotein transport activity at the human blood-brain barrier with positron emission tomography. *Clin Pharmacol Ther.* 2005;77:503–514.
28. Dehdashti F, Wu N, Ma CX, Naughton MJ, Katzenellenbogen JA, Siegel BA. Association of PET-based estradiol-challenge test for breast cancer progesterone receptors with response to endocrine therapy. *Nat Commun.* 2021;12:733.
29. Wang Y, Ayres KL, Goldman DA, et al. ^{18}F-fluoroestradiol PET/CT measurement of estrogen receptor suppression during a phase I trial of the novel estrogen receptor-targeted therapeutic GDC-0810: using an imaging biomarker to guide drug dosage in subsequent trials. *Clin Cancer Res.* 2017;23:3053–3060.
30. Mankoff DA, Eary JF, Link JM, et al. Tumor-specific positron emission tomography imaging in patients: [^{18}F] fluorodeoxyglucose and beyond. *Clin Cancer Res.* 2007;13:3460–3469.
31. Qu W, Oya S, Lieberman BP, et al. Preparation and characterization of l-[5-^{11}C]-glutamine for metabolic imaging of tumors. *J Nucl Med.* 2012;53:98–105.
32. Cohen AS, Grudzinski J, Smith GT, et al. First-in-human PET imaging and estimated radiation dosimetry of l-[5-11C]-glutamine in patients with metastatic colorectal cancer. *J Nucl Med.* 2022;63:36–43.
33. Michaud L, Beattie BJ, Akhurst T, et al. ^{18}F-fluciclovine (^{18}F-FACBC) PET imaging of recurrent brain tumors. *Eur J Nucl Med Mol Imaging.* 2020;47: 1353–1367.
34. Debus C, Afshar-Oromieh A, Floca R, et al. Feasibility and robustness of dynamic ^{18}F-FET PET based tracer kinetic models applied to patients with recurrent high-grade glioma prior to carbon ion irradiation. *Sci Rep.* 2018;8:14760.
35. Shoup TM, Olson J, Hoffman JM, et al. Synthesis and evaluation of [^{18}F]1-amino-3-fluorocyclobutane-1-carboxylic acid to image brain tumors. *J Nucl Med.* 1999; 40:331–338.